Escape time, relaxation, and sticky states of a softened Henon-Heiles model: Low-frequency vibrational mode effects and glass relaxation

J. Quetzalcóatl Toledo-Marín and Gerardo G. Naumis*

Departamento de Sistemas Complejos, Instituto de Física, Universidad Nacional Autónoma de México (UNAM), Apartado Postal 20-364, 01000 México, Distrito Federal, México

(Received 27 October 2017; revised manuscript received 24 January 2018; published 6 April 2018)

Here we study the relaxation of a chain consisting of three masses joined by nonlinear springs and periodic conditions when the stiffness is weakened. This system, when expressed in their normal coordinates, yields a softened Henon-Heiles system. By reducing the stiffness of one low-frequency vibrational mode, a faster relaxation is enabled. This is due to a reduction of the energy barrier heights along the softened normal mode as well as for a widening of the opening channels of the energy landscape in configurational space. The relaxation is for the most part exponential, and can be explained by a simple flux equation. Yet, for some initial conditions the relaxation follows as a power law, and in many cases there is a regime change from exponential to power-law decay. We pinpoint the initial conditions for the power-law decay, finding two regions of sticky states. For such states, quasiperiodic orbits are found since almost for all components of the initial momentum orientation, the system is trapped inside two pockets of configurational space. The softened Henon-Heiles model presented here is intended as the simplest model in order to understand the interplay of rigidity, nonlinear interactions and relaxation for nonequilibrium systems such as glass-forming melts or soft matter. Our softened system can be applied to model β relaxation in glasses and suggest that local reorientational jumps can have an exponential and a nonexponential contribution for relaxation, the latter due to asymmetric molecules sticking in cages for certain orientations.

DOI: 10.1103/PhysRevE.97.042106

I. INTRODUCTION

Relaxation processes are abundant in the universe. In fact, if one were to take a snapshot of the universe, one would see that only a small number of physical systems are in equilibrium, while the rest are either in steady states or relaxing towards equilibrium. All the same, it is not clear how relaxation processes depend upon the energy landscape [1–6]. It is of common knowledge that this is due to mainly two contributions, one being the energy landscape complexity itself, and the other being the interaction with the surroundings of the system. However, even if we only consider the complexity of the energy landscape, one would find that the system has an intermittent chaotic behavior. In this way, the deterministic feature lacks meaning, similar to what happens in stochastic processes [7]. Furthermore, what we call stochastic behavior and chaotic behavior seems to be two faces of the same coin [8]. In this sense, Alvaro *et al.* in Ref. [9] are able to establish this sort of correspondence for two particular well-known stochastic models.

In order to guarantee that a given system under study will tend to an equilibrium state, one usually imposes detailed balance or assumes the conditions are fulfilled for the fluctuation-dissipation theorem or the equipartition theorem. However, this is not obvious when going from a classical mechanical approach to a statistical mechanical one. As it is well known, this is what Fermi, Pasta, and Ulam investigated back in 1954, by considering a chain of nonlinear oscillators. What they found is quite long to summarize here (see Ref. [10]). However, as one would expect, this relaxation depends strongly on the mode coupling, i.e., the nonlinear terms. In fact, Ponno in Ref. [11] presents some estimates on how the energy is transferred from one mode to another, as well as the characteristic relaxation time, which is proportional to the number of oscillators. What is even more interesting is that this energy sharing starts in the low vibrational modes due to resonances, which was first pointed out in Ref. [12]. This is because the dispersion relation for the low vibrational modes is linear and the frequencies are linearly dependent. Then each mode will resonate with their mode-coupling term. Here lies the importance of the low vibrational modes.

Nonetheless, the relaxation mechanism, in particular, in supercooled liquids has proven to be a very complex one. In fact, the general features of supercooled liquids still lack of a scientific explanation, because of the complex nature of it. On the one hand, the problem is difficult because the harmonic approximation breaks down for the Hamiltonian at long-time scales, which are relevant to describe the relaxation and viscosity properties of glassy melts [1]. On the other hand, the glass transition is a nonequilibrium transition problem where the system does not have long-range order. These arguments are just the tip of the iceberg that give foundation to why this problem is a very complex one. Despite the amount of research focused on it (see Refs. [13–20] and in particular [21] and references therein), there is not too much of a consensus and rather different points of view. To spice things up a little, experiments and simulations have not yet met in the sense that it

*naumis@fisica.unam.mx

takes too much computational time to drive the system toward a region near the glass transition temperature. Yet attention should be paid to recent simulations [22].

One of the questions that arise in this phenomenon is how the glass transition temperature, T_g, is related to the composition of the glass former [23,24]. Rigidity theory [25–29] gives some insight on this aspect in a qualitative manner, and works quite well in the case of chalcogenide glasses. Another rather interesting feature in supercooled liquids is the viscosity behavior during a quench. As is well known, viscosity is a property that depends upon relaxation, i.e., the time that the system takes in order to leave a basin of the energy landscape and produce a structural relaxation. Depending on this behavior, the supercooled liquid is classified as a strong one if it follows the Arrhenius equation and as a fragile one if it follows the Vogel-Fulcher-Tamman equation [3,21]. The fragility or nonfragility of a supercooled liquid is related with the glass forming tendency in the sense that strong supercooled liquids have a strong glass forming tendency such that do not require large quenches in comparison with fragile ones, which are poor glass formers. Thus, the glass-forming tendency is clearly related with the time relaxation of the system.

It is well known that there is a correlation between the glass transition temperature, T_g, and the cooling rate. Quite recently, Lerner *et al.* in Refs. [30,31] have shown that the statistics and localization of low-frequency vibrational modes depend upon the cooling rate. Thus, there lies a trichotomy, namely, glass transition, relaxation, and low-frequency vibrational modes. In a series of previous papers, we have discussed how these are related in a very natural way [32–37]. In fact, rigidity theory has allowed us to rationalize how they are interrelated [38]. In their rigidity theory, Phillips, and later Thorpe, consider covalent bonding as a mechanical constraint [25,26]. In this sense, one may summarize the main feature of this theory as follows. When the number of bond constraints equals the number of degrees of freedom, the glass forming ability is optimized, i.e., producing glass requires the slowest cooling rate. In this situation, the mean coordination number equals the critical percolation coordination number, i.e., domains of floppy modes (zero-frequency modes) and rigid modes coexist. As the mean coordination number decreases, which may be tuned by varying the chemical composition, floppy mode domains grow while rigid mode domains disappear. As floppy modes increase in number, the glass formation is more difficult. It is important to remark that at the rigidity percolation threshold, the fragility has a minimum, hence not only the increase of floppy modes leads to a more fragile glass [32,39–42]. In addition, at the rigidity threshold not always floppy modes and rigid modes coexist, for instance, for jamming transition the low fluctuation on coordination suppresses the formation of localized floppy modes. For chalcogenide glasses, it is believed that the increase of fragility is due to the explosive elastic energy of overconstrained stressed bonds, which helps crystallization [25,32].

However, there are no general models to deal with the nonlinear regime, which is the one that is interesting for glass transition. With these ideas in mind, here we study and present our findings on the relaxation behavior when we decrease the frequency of the normal modes toward zero, i.e., floppy modes, in the case of a chain formed by three nonlinear oscillators, which when expressed in the coordinates that diagonalize the linear part yields the Henon-Heiles potential. This potential is a particular case of the Fermi-Pasta-Ulam (FPU) model, in which it is known that low-frequency modes are responsible for relaxation [43–46]. This has been made by adding second neighbors, disorder, and quasiperiodicity [44,45,47,48]. The advantage of the Henon-Heiles model is that it contains the minimal ingredients to understand the effects of nonlinearity. In that sense, here we provide a minimal model to understand how low-frequency modes impact the escape time and relaxation of the system.

It is worthwhile mentioning that the Henon-Heiles potential has been widely studied [49–54]. Concerning the escape dynamics, it has been observed that the phase space escape flow follows an exponential law connected to chaotic dynamics, whereas in nonchaotic dynamics the phase space escape follows a power law. Using simple arguments, Zhao *et al.* [54] obtain the exponential law, which they then compare successfully with their simulations in the case of chaotic dynamics, with a small threshold energy. Bauer and Bertsch [55] also obtained the exponential law before Zhao *et al.* Furthermore, from a heuristic and retrospective approach they obtain the power law. However, one of the results in the present work is the crossover between exponentially decaying law and power law, which is not seen in Ref. [54] because they consider smaller threshold energies and short times.

The paper is organized as follows. In the following section we present the model and its features. In Sec. III we present the results obtained from the simulations and how the exponential relaxation is affected by low-frequency vibrational modes. In Sec. IV we study special states that are sticky, which instead present a power-law relaxation. In Sec. V we apply the model to relaxation in glasses. Finally, in Sec. VI we discuss these results.

II. SOFTENED HENON-HEILES MODEL

Let us consider a chain consisting of three masses joined by nonlinear springs and periodic conditions. Thus, the Hamiltonian is

$$H = \sum_{i=1}^{3} \frac{1}{2m} \vec{P}_i^2 + \frac{1}{2} k_{i+1,i} (\Delta Q_{i+1,i})^2 + \frac{\gamma}{3} (\Delta Q_{i+1,i})^3, \quad (1)$$

where $\Delta Q_{i+1,i} = Q_{i+1} - Q_i$ and $k_{i+1,i}$ is the spring stiffness between masses i and $i+1$. Furthermore, let us introduce the control parameters α and β in the stiffness such that $k_{21} = k$, $k_{21}\beta = k_{13}$, and $k_{32} = \alpha k_{21}$.

One of the eigenvalues of dynamic matrix **D** is always zero and corresponds to the center of mass motion, while the other two depend upon α and β [56]. However, as was stated in Sec. I, we are interested in studying the low vibrational dynamics relaxation process. In this sense, it happens that ω_x becomes zero only when $\alpha = \beta = 0$ while ω_y becomes $\sqrt{2}$. Thus, here we consider $\alpha = \beta$ and without loss in generality we assume $k = 1$. Therefore, the eigenvalues become

$$\omega_x^2 = 3\beta, \quad \omega_y^2 = 2 + \beta, \quad \omega_z^2 = 0. \quad (2)$$

Finally, by expressing the nonlinear term in terms of the normal coordinates and momenta we obtain

$$H = \frac{1}{2}\left(p_x^2 + p_y^2\right) + \frac{1}{2}\left(\omega_x^2 x^2 + \omega_y^2 y^2\right) - \frac{3\gamma}{2^{1/2}}\left(\frac{1}{3}y^3 - x^2 y\right), \tag{3}$$

which corresponds to two particles interacting via a Henon-Heiles-type potential [53].

Furthermore, let us do the following rescalings:

$$y \to \frac{2^{1/2}}{\gamma}y, \quad x \to \frac{2^{1/2}}{\gamma}x, \quad t \to t/3^{1/2}, \quad H \to \frac{6}{\gamma^2}H. \tag{4}$$

This gives the scaled Hamiltonian:

$$H = \tfrac{1}{2}\left(p_x^2 + p_y^2\right) + \tfrac{1}{6}\left(\omega_x^2 x^2 + \omega_y^2 y^2\right) - \left(\tfrac{1}{3}y^3 - x^2 y\right), \tag{5}$$

and the Hamilton equations are

$$\begin{aligned} \dot{x}_i(t) &= p_i(t), \quad x_i = \{x, y, z\} \\ \dot{p}_x(t) &= -x(t)[\beta + 2y(t)], \\ \dot{p}_y(t) &= -\tfrac{1}{3}(2+\beta)y(t) + [y(t)]^2 - [x(t)]^2. \end{aligned} \tag{6}$$

The resulting model is a softened Henon-Heiles system, since by making $\beta \to 0$, ω_x goes to zero, resulting in a floppy mode. Thus, β is a control parameter that allows us to reduce the stiffness of the low-frequency vibrational modes. This results in a lowering of two saddle points height. In the top panel of Fig. 1 we have depicted the isopotential for a fixed β and different energies. We also show the three saddle points (red dots) and the local minimum for the potential (black dot) where the potential energy is zero. In the bottom panel of Fig. 1 we may appreciate how the height of the saddle points P_1 and P_2 are the same and smaller than P_3. Moreover, in Fig. 2 we have plotted the saddle points height vs β. When $\beta = 0$ the potential barriers located at P_1 and P_2 drop to zero, while the other barrier drops to $\simeq 0.05$ (see Fig. 2).

In the case for which $\beta = 1$, all saddle points have the same height. This Hamiltonian corresponds to the model used by Hénon and Heiles to study the motion of a star in a galaxy with cylindrical symmetry [49]. For a certain choice of parameters it has been proven to be an integrable problem [50], but it is not in general. Moreover, numerical results suggest that when the energy of the system is $E < 1/12$, the system is nonchaotic and nonergodic, yet above this energy the region with chaotic behavior in phase space increases with the energy up until $E = 1/6$ where the whole phase space is chaotic and which is also saddle point's height [53,54].

In this way, it seems that as the energy increases the dynamics become chaotic and ergodicity is established. However, in this work we show that this is not always the case for the softened model. Actually, as the energy increases, there are certain islets in the phase space for which quasiperiodicity is established. This is done in the following section.

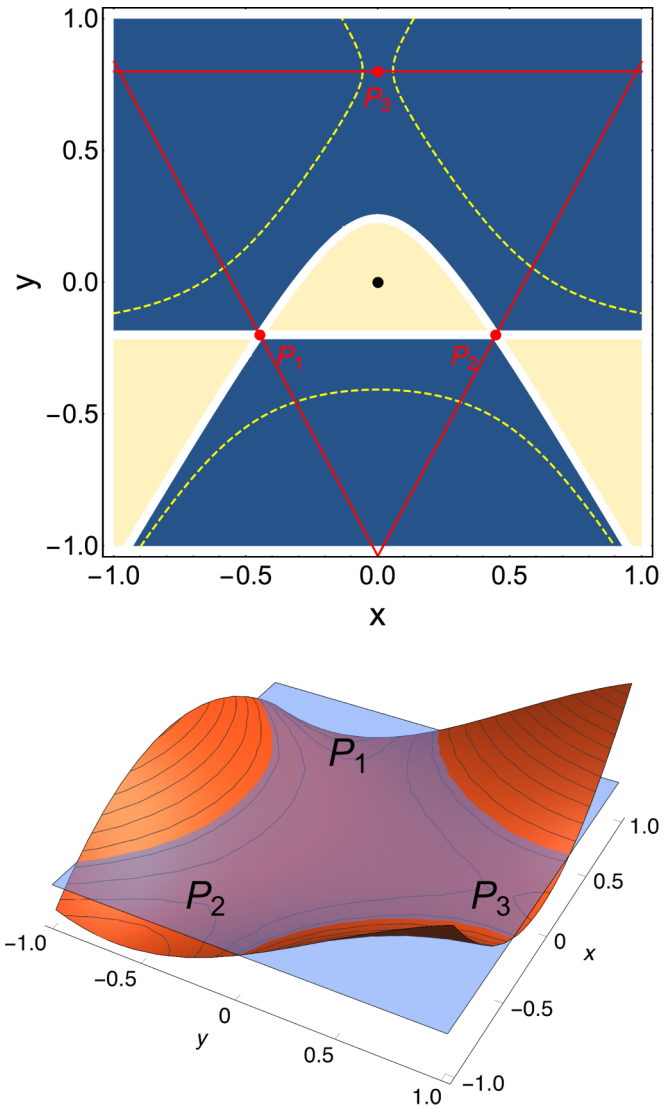

FIG. 1. Energy landscape showing an isopotential with $\beta = 0.4$. (Top) The dashed line correspond to the isopotential with energy, $\Delta E = 0.07$, above the lower saddle points height (yellow) while the inner softened triangle corresponds to $\Delta E = 0$. Each line of the red triangle goes through a saddle point and has the direction of the eigenvector corresponding to the positive eigenvalue of the Hessian matrix in the corresponding saddle point. (Bottom) Here we show a three-dimensional (3D) plot of the potential. The transversal plane corresponds to $\Delta E = 0.07$.

III. RELAXATION PROPERTIES OF THE SOFTENED HENON-HEILES MODEL

In this section we present the results obtained from solving numerically the Hamiltonian equations [Eqs. (6)]. We first fixed β and the energy, ΔE, above the lower saddle points height (see Fig. 1), then we took $N = 16000$ randomly chosen initial conditions, i.e., linear moment orientation and position, given the fixed energy. Then we let them evolve and we studied the distribution of their escape time, i.e., the time taken to escape the well through any of the exit channels denoted as P_1, P_2, and P_3 (see Fig. 1). We did this for different values of the parameters β and ΔE, which we present in Fig. 3 (the blue

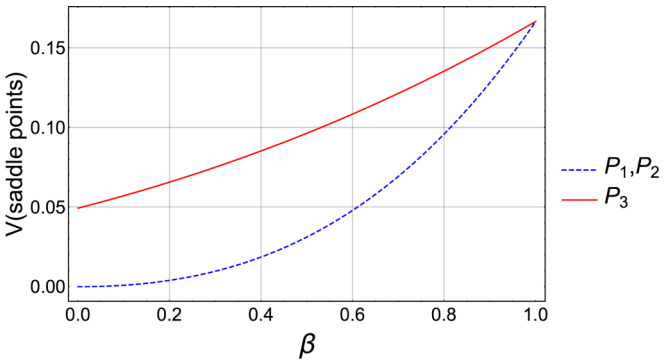

FIG. 2. Plot of the saddle-point heights as a function of β. The blue dashed curve corresponds to the saddle-point height at P_1 and P_2, while the red continuous curve corresponds to the saddle-point height at P_3 (see Fig. 1).

line in Fig. 3 corresponds to the energy difference between the upper saddle point and the lower saddle points, i.e., for a given fixed β when ΔE is under the blue curve there are two exit channels, namely, P_1 and P_2; while when ΔE is above the blue curve, there are three exit channels).

In Figs. 4, 5, 6, and 7 we present the population $N(t)$ inside the well as a function of time in linear-log and log-log plots. We also present the potential contour corresponding to each of the values for ΔE for a fixed β. Rather than using legends in each of the plots, we used instead the same colors, i.e., the red curves in the potential contour plot and in the $N(t)$ vs t correspond to the same value of ΔE, which we show in Fig. 3. The first thing one may notice is that, in general, the escape flow at a given time follows an exponential decay. However, there are some values of β and ΔE for which the escape flow at a given time has a crossover unto a power-law decay and sticky states appear, but we will come back to this later.

Notice that for small t it seems that $N(t) \sim \exp(-\alpha t)$. In Fig. 8 we present the values of α as a function of β and ΔE, obtained by fitting the curves in Figs. 4, 5, 6, and 7 in the short-time regime [56]. The dashed line divides the scenario

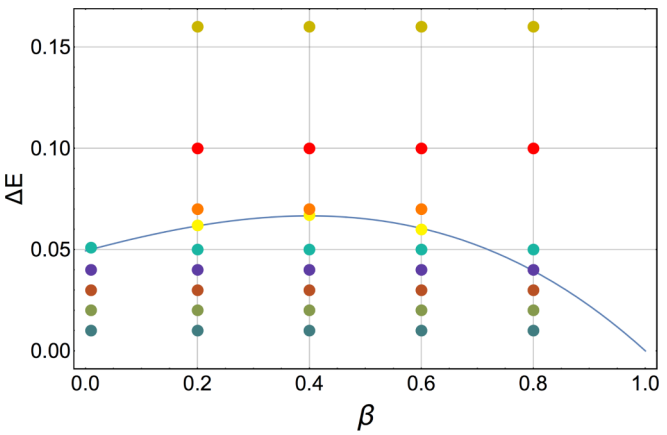

FIG. 3. Sets of parameters $(\beta, \Delta E)$ used in our simulations to study relaxation. Points of the same color have the same energy ΔE above the lowest saddle points. The blue curve corresponds to the energy difference between the high and low saddle points, i.e., for ΔE under the blue curve there are two exit channels, namely, P_1 and P_2 and for ΔE above the blue curve, there are three exit channels.

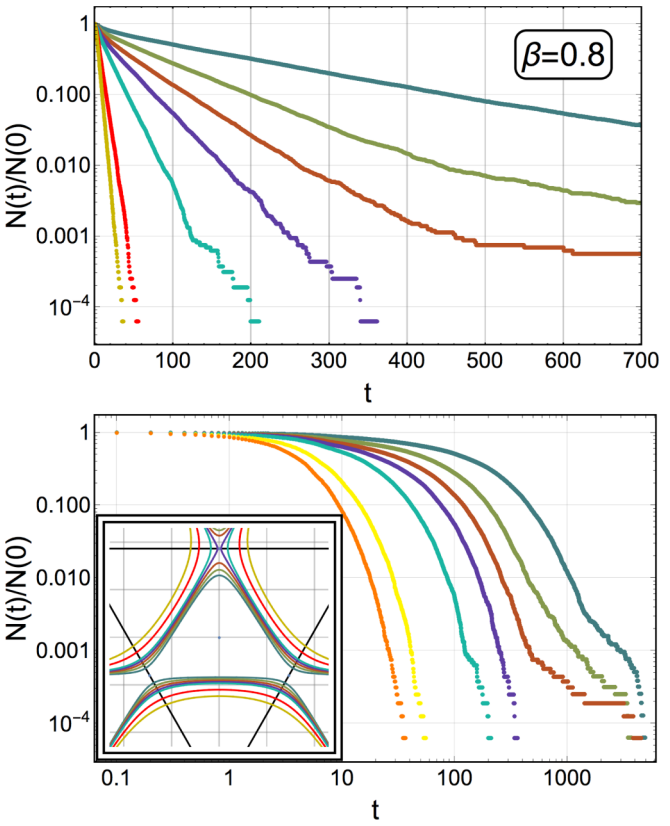

FIG. 4. For $\beta = 0.8$: (Top) The population in the potential at time t in a log-linear plot, for different energies as indicated in the color code of Fig. 3. (Bottom) The population in the potential at time t in log-log. (Inset) The isopotential for different values of ΔE (see Fig. 3).

in which there are only two exit channels (which correspond to the two lower saddle points) from the scenario where there are three exit channels (see Fig. 1).

To understand this exponential decay behavior for the unsoftened Henon-Heiles model ($\beta = 1$), first Bauer and Bertsch and then Zhao *et al.* (see Refs. [54,55]) used simple rather clever arguments. They considered that all initial conditions contained in the energy landscape well would flow out and assumed that the population change rate equals the flux with momentum orientation between $-\pi/2$ and $\pi/2$ relative to the normals of the exit channels line. Hence

$$\frac{dN(t)}{dt} = -N(t)\rho \int_{-\pi/2}^{\pi/2} d\theta \int_{r_0}^{r_1} dl |\vec{v}(x,y)| \cos\theta, \qquad (7)$$

where $\rho = 1/2\pi S(\Delta E)$ is the distribution of the variables (x, y, θ) and $S(\Delta E)$ is the area of the well. The integral goes over the opened exit channel lines and, the points r_0 and r_1 correspond to the classical return points at these opened exit channel lines. In the case where $\beta = 1$, all exit channels are identical. Then, integrating over the exit channel P_3 and multiplying by three yields

$$\frac{dN(t)}{dt} = -\frac{\sqrt{3}\Delta E}{S(\Delta E)} N(t). \qquad (8)$$

Hence, $N(t) \sim e^{-\alpha t}$, with $\alpha = \sqrt{3}\Delta E / S(\Delta E)$.

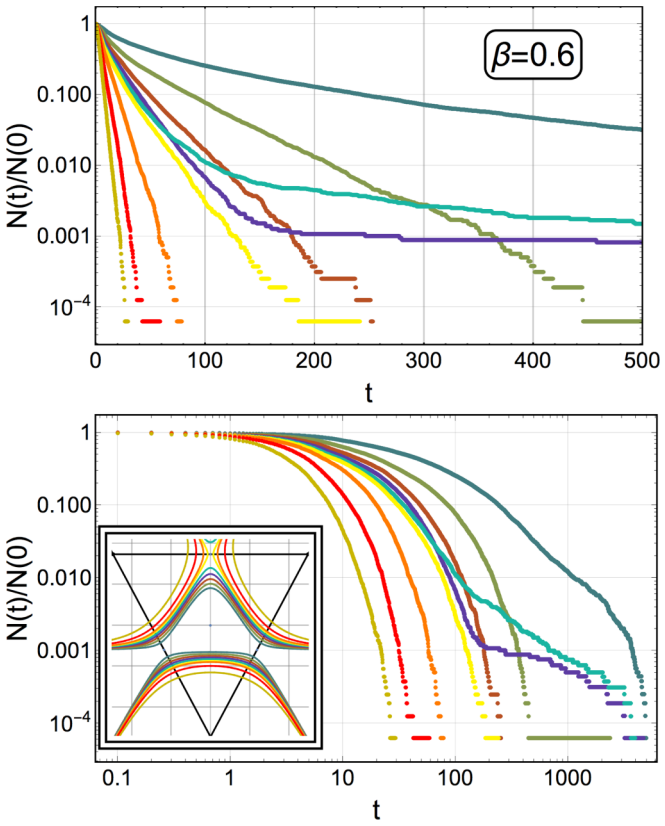

FIG. 5. For $\beta = 0.6$: (Top) The population in the potential at time t in log-linear, for different energies as indicated in the color code of Fig. 3. (Bottom) The population in the potential at time t in log-log. (Inset) The isopotential for different values of ΔE (see Fig. 3).

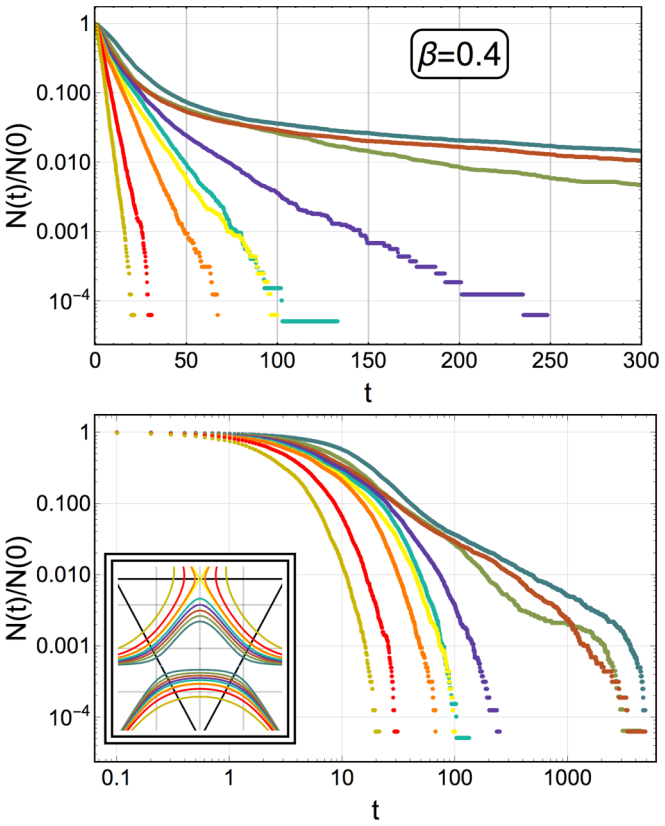

FIG. 6. For $\beta = 0.4$: (Top) The population in the potential at time t in log-linear, for different energies as indicated in the color code of Fig. 3. (Bottom) The population in the potential at time t in log-log. (Inset) The isopotential for different values of ΔE (see Fig. 3).

In the softened Henon-Heiles model, the exit channels P_1 and P_2 are identical and different from P_3. Following this same idea, we determined $\alpha(\beta, \Delta E)$ by estimating the escaping flux numerically from Eq. (7), but evaluated for the open channels for a given energy where

$$|v(x,y)| = \left\{2\left[\Delta E + \tfrac{1}{12}\beta^2(1+\beta) - \tfrac{1}{6}(3\beta x^2 + (2+\beta)y^2) + \left(\tfrac{1}{3}y^3 - x^2 y\right)\right]\right\}^{1/2}. \quad (9)$$

The first two terms on the right-hand side of Eq. (9) are simply the energy above the lower saddle points and the lower saddle points energy height. The third term in the right-hand side of Eq. (9) is the softened Henon-Heiles potential. The classical returning points as well as the area of the wells, $S(\Delta E)$, were also determined numerically for different values of ΔE.

These results can be compared with the actual fitting of α obtained from the numerical results of $\log N(t)$ for small t, as obtained in Figs. 4, 5, 6, and 7. In Fig. 9 we compare both methods, namely, the blue points correspond to the fitting methods while the orange curves correspond to the numerical flux estimation method. The discontinuity around $\Delta E \approx 0.05$ corresponds to the threshold energy where the exit channel P_3 is available. We should clarify that the orange curves were obtained by interpolating numerical results, i.e., no analytical equation was obtained. One may appreciate how this heuristic approach works quite well for small ΔE, not so much for when the flow may come out through the upper channel, i.e., P_3. This has to do with the fact that in this regime, not all initial conditions in configurational space flow out of the basin, as we will show later.

From Figs. 8 and 9 is clear that the relaxation time is decreased as the stiffness of the model is reduced, since in general α grows as β is reduced for a fixed energy. This is explained in general by two effects. The first is a reduction of the energy barrier heights along the softened normal modes (see Fig. 2), and the second is a widening of the opening channels.

IV. POWER LAW RELAXATION AND STICKY STATES

To have a better grip and to qualitatively differentiate which conditions flow out following an exponential decay from the region, which flows out following a power law, we fixed $\beta = 0.4$ and $\Delta E = 0.02$ and solved numerically the Hamilton Eqs. (6) for $N \simeq 5 \times 10^4$ different initial conditions, i.e., (x, y, θ). In the top panel of Fig. 10 we have plotted ∼50% of the studied initial positions that flow out first, i.e., we plot the configurational space region that corresponds to the exponential decay regime of $N(t)$, and we have colored each point according to their initial moment orientation. We also did this for the initial conditions that flow out the slowest, corresponding to the power-law regime of $N(t)$, and we show

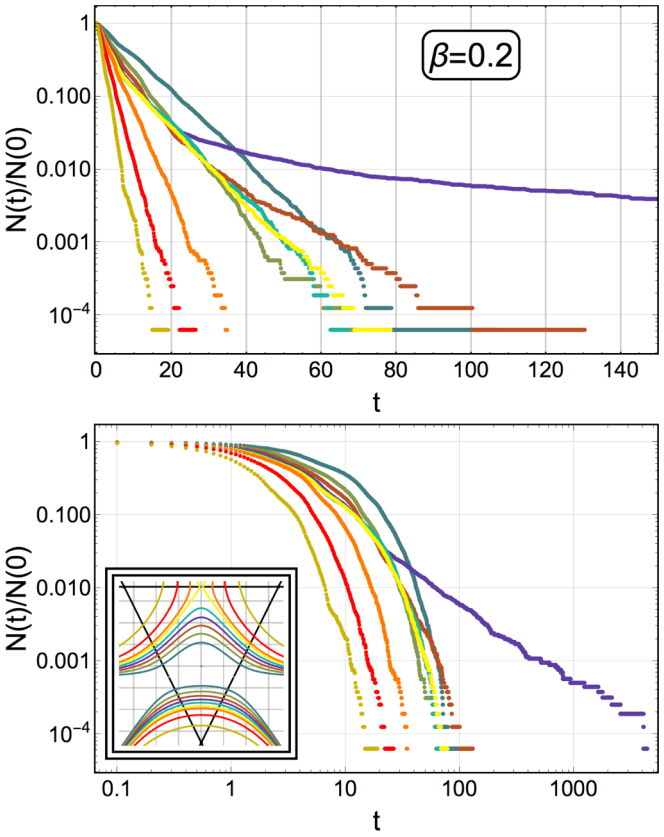

FIG. 7. For $\beta = 0.2$: (Top) The population in the potential at time t in log-linear, for different energies as indicated in the code of Fig. 3. (Bottom) The population in the potential at time t in log-log. (Inset) The isopotential for different values of ΔE (see Fig. 3).

this in the bottom panel of Fig. 10. There are several features we may extract from this. First, notice that the conditions that flow out first are those with an initial moment orientated toward the exits. Yet, there are some initial positions that define two regions, namely, region I and region II (see top panel in Fig. 10), which does not flow out during the

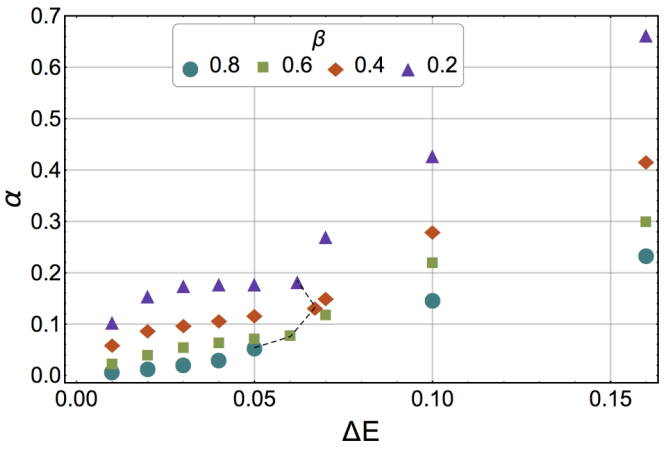

FIG. 8. $\alpha(\beta, \Delta E)$ obtained numerically by solving the Hamilton equations (6). The dashed line separates the region where the exit channel corresponding to the saddle point P_3 is forbidden (left) and the region where it is accessible (right).

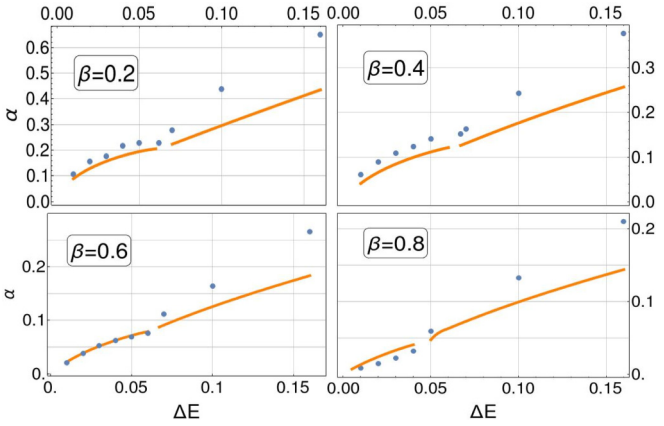

FIG. 9. $\alpha(\beta, \Delta E)$ obtained from numerically solving the Hamilton Eqs. (6) (blue dots) and by considering the initial conditions escape flux [see Eq. (7)] (yellow lines). The regime change around $\Delta E \approx 0.05$ corresponds to the threshold where the exit channel P_3 is available.

exponential decay regime no matter what their initial moment orientation is. This is further verified in the bottom panel of Fig. 10 from which we may qualitatively appreciate a density gradient in the y direction for $y > 0$ and in the $-y$ direction for $y < 0$.

Also notice that the bulk of the initial positions that flow out slowly is concentrated in a vicinity of $x \simeq 0$. However, there is clearly an overlap in this vicinity with the initial positions that exit quite fast. For this reason, in Fig. 11 we have plotted in the top panel the initial condition coordinate x and the initial moment orientation θ for 50% for the initial conditions that flows out first, while in the bottom panel of Fig. 11 we plotted the initial condition coordinate y and the initial moment orientation θ of the slowest flowing initial conditions. In both plots the color is a function of the exit time, i.e., red corresponds to the smallest exiting time while navy blue corresponds to the largest exiting time. Notice that from the top panel of Fig. 11 one may appreciate fairly well that the configurational space region that flows out first is the one next to the left (right) exit channel and have initial moment orientation between 2.3 and $3\pi/2$ (4.5 and $2\pi + 1$), then the initial conditions region that follows has an initial moment orientation contained in these intervals but with smaller absolute value of the initial position coordinate x, in other words, the initial moment orientation still corresponds to that directed toward one of the exits channels. Now, the initial conditions region that follows has an initial moment orientation in the vicinity of $\pi/2$ and is distributed around $x \pm 0.3$. This means that this initial conditions region collides with the potential barrier before being able to flow out.

Now, from the bottom panel in Fig. 11 we may appreciate that the initial conditions region that takes the longest to flow out is distributed all over the classically permitted interval in the y axis but with either $\pi/2$ or $3\pi/2$ as the value of the initial moment orientation. All this suggests that the region that takes the longest to flow out corresponds to oscillating trajectories in the y direction and in a quasiperiodic manner with $x(t) \simeq 0$, i.e., sticky orbits appear.

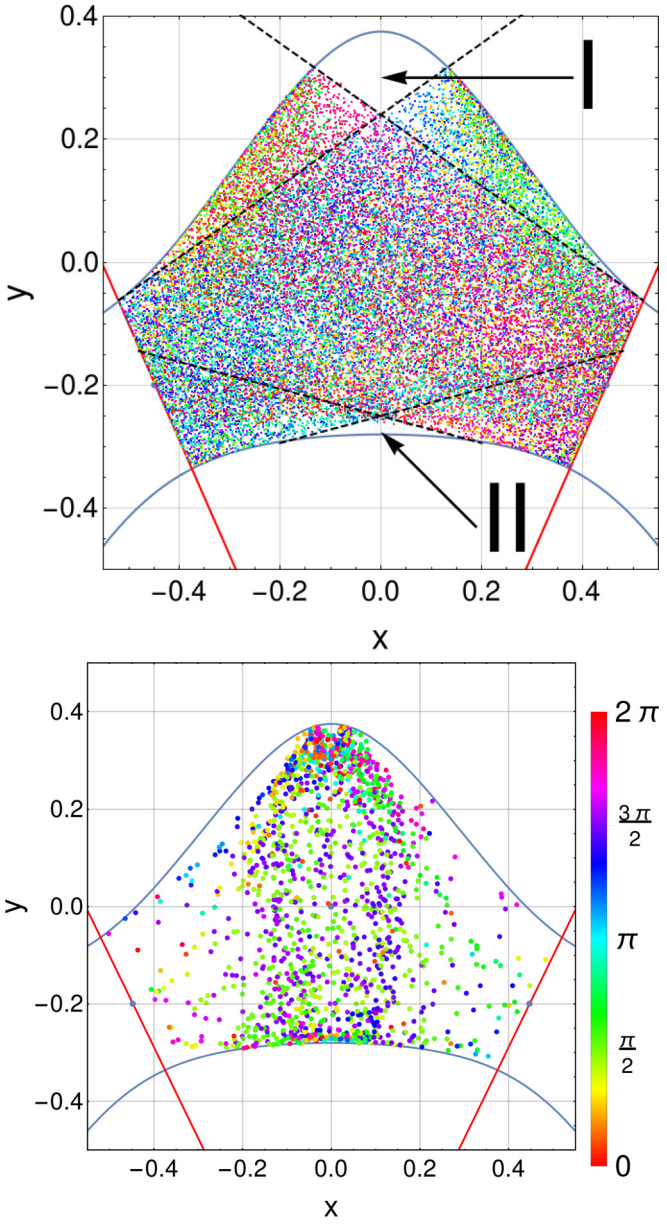

FIG. 10. Escape decay regimen as a function of the initial position for $\beta = 0.4$ and $\Delta E = 0.02$. The coloring corresponds to the initial moment orientation with respect to the horizontal (see legend). (Top) Particles that escape under the exponential decay regime. The black dashed lines are an eye guideline to indicate the conelike regions of particles with initial moment orientation directed towards one of the exits, and also indicate the regions I and II were particles there take longer to escape no matter what their initial moment orientation is. (Bottom) Particles that escape under the power-law regime as a function of the initial positions. The isopotential curve is indicated in blue while the exits of the potential basin is indicated by lines.

Going one step further, in Fig. 12 we show a Poincaré section for one of the initial conditions that takes a long time to flow out, obtained in the case of $\beta = 0.4$ and $\Delta E = 0.02$. Clearly, this type of section corresponds to a quasiperiodic trajectory. Eventually, the small deviations amplify and the trajectory escapes the well.

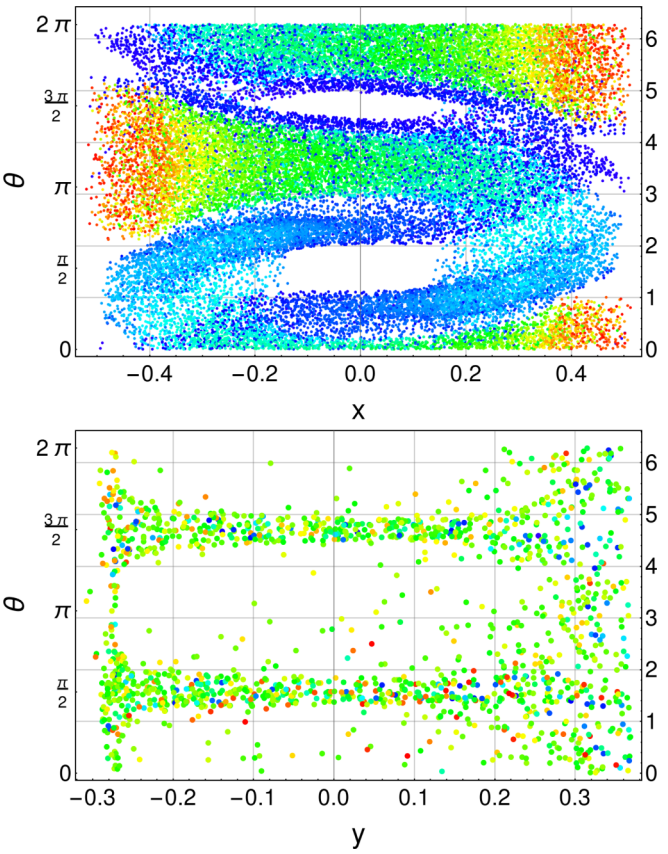

FIG. 11. Decay regime as a function of the initial position x and initial moment orientation θ in the case of $\beta = 0.4$ and $\Delta E = 0.02$. (Top) Particles that escape under the exponential decay regime. (Bottom) Particles that escape under the power-law regime. The coloring corresponds to the time taken to escape, such that red is short exit times and navy blue is for large exit times (see legend).

V. APPLICATION TO GLASSES

The previous results can be put in many ways into the context of glasses. First, the softening of the energy barriers due to flexible modes observed in the previous model can

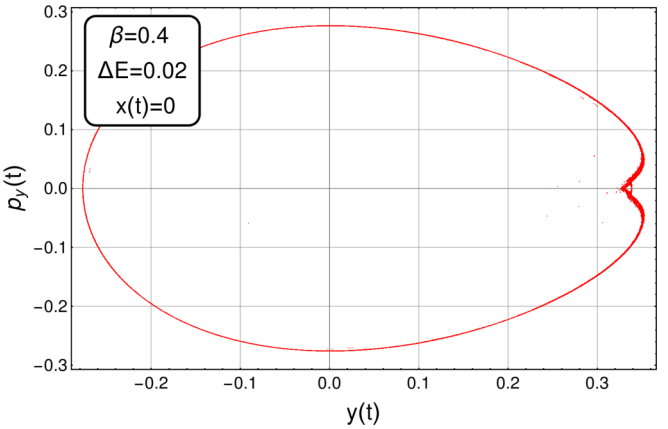

FIG. 12. Poincaré map for $\beta = 0.2, \Delta E = 0.04$, and some initial condition for which the particle takes a long time to exit the basin, corresponding to a sticky state.

be generalized for glasses. To this end, consider N atoms described by a pairwise potential, say, $V(\{x_i\})$ where $\{x_i\}$ is the set of generalized normal coordinates expanded around a meta-stable state with $i = 1, \ldots, 3N$ and let us assume that $V(\{0\}) = 0$, hence

$$V(\{x_i\}) = \frac{1}{2}\sum_{i=1}^{3N} \omega_i^2 x_i^2 + V_{NL}(\{x_i\}). \tag{10}$$

Here $V_{NL}(\{x_i\})$ denotes the nonlinear part of the potential. In general, floppy modes occur by lowering interactions, usually by more than an order of magnitude. For example, in pure Se glass 1/3 of the modes are floppy since there are almost no energy cost in changing the dihedral angle of the Se-Se-Se bonds [25,57]. Yet weaker Van der Waals forces produce a blue shift of the floppy mode from zero frequency [38,57]. Stiffness can be increased by adding cross-linking modifiers such as Ge, which add stronger interactions [25]. Floppy modes can also be produced by reducing sizes of some atoms when using Lennard-Jones potentials [34,35]. Thus, if we were to loosen the stiffness of a fraction f of the normal modes, i.e., decrease ω_j with $j = 1, \ldots, 3Nf$, in general, one would expect a variation in the no-linear part of the potential in the sense that it will ultimately depend on the kind of potential that describes a given supercooled liquid and the physical way in which one modifies the stiffness of the normal modes. Since the details depend upon the particular potential, here we adopt a worst-case scenario, i.e., we may assume that the nonlinear part of the potential is kept fixed when the stiffness is loosened. Therefore, we denote the potential with a fraction f of floppy modes as $V_F(\{x_i\})$, such that

$$V_F(\{x_i\}) = \frac{1}{2}\sum_{i=1}^{3N(1-f)} \omega_i^2 x_i^2 + \frac{1}{2}\sum_{j=1}^{3Nf} \lambda_j \omega_j^2 x_j^2 + V_{NL}(\{x_j\}), \tag{11}$$

where we have denoted the fraction of floppy normal modes as $\sqrt{\lambda_j}\omega_j$ and $0 < \lambda_j < 1$. Then, notice that

$$V_F(\{x_i\}) = V(\{x_i\}) - \frac{1}{2}\sum_{j=1}^{3Nf}(1-\lambda_j)\omega_j^2 x_j^2, \tag{12}$$

which implies that

$$V_F(\{x_i\}) \leqslant V(\{x_i\}), \tag{13}$$

since the second term in Eq. (12) is always positive. Thus, in general the energy barrier height decreases in the direction of floppy modes in comparison to rigid modes, and one expects relaxation in the direction of floppy modes. It is clear that this general behavior is what lies in our soft Henon-Heiles model, which is the extreme case of two degrees of freedom (fixing the center of mass). Yet even this two degrees of freedom model can be used to understand some features of glass relaxation.

For example, recently there has been a lot of theoretical interest in the β relaxation (not to be mistaken with the β parameter in our model) or Johari-Goldstein relaxation for glass-forming materials, since it has been revealed its connection with the glass transition [58]. This phenomenon becomes visible below the melting temperature. Yet, the origin of this has generated controversy [59–61], but it seems quite likely that this relaxation is concerned with the small-amplitude rotational jump motion of molecules [62–64]. In Ref. [60], Tanaka proposed a two-order parameter phenomenological model for rigidity and glass relaxation, which is based on local fluctuations of reorientational jumps, identified with the β relaxation. These fluctuations are observed within rigid metastable islands. The relaxation of these rigid islands is also known as the α-relaxation process (not to be confused with the α parameter in our model), which slows down when reaching the glass transition temperature upon cooling. This is why the β relaxation becomes visible below the melting temperature where the α-relaxation time starts to pick up, and molecules start being caged. The origin of the α relaxation has also generated controversy in glass-forming liquids and it seems to be one of the key ingredients of the glass transition. Both, α and β relaxations seems to be important in the glass transition, since the first one is associated with a long-range ordering while the second one with a short-range ordering, and the competition between these two creates an energetic frustration causing the glass transition. Now, in most glasses, there happens to be an overlap between the α relaxation and the β relaxation. Much dissent has caused the fact that it is not clear whether this overlap is for the most part the α-relaxation mode excess wing or the so-called slow-β-relaxation mode. Here lies the main purpose of Tanaka's two-order parameter mode [60].

In this sense, our model may be applied to the Tanaka's rigidity relaxation model. Within this model, there are local fluctuations with reorientational jumps [60]. Consider three-dimensional asymmetrical molecules caged by a rigid surrounding metastable island. For each molecule, the rotational state can be described by two Euler angles coordinates, the polar angle η and the azimuthal angle ϕ. We associate the coordinates x and y of our softened Henon-Heiles model to these angles. Due to the asymmetry of the molecule, the interactions with the rigid cage will lead to different elastic constants for each Euler angle, and thus Eq. (3) can be used as a model. A reorientational jump will be associated with an exit of the model's central basin. Since in our model any given initial condition exits the basin once the momentum orientation θ points outwards through any of the available exit channels, then the characteristic β-relaxation time τ is proportional to the mean exit time in our model. In the case where the flux method applies, the mean time for a reorientational jump is simply the inverse of α, thus $\tau \sim 1/\alpha$. The exponential law decay is in agreement with the experimental observed Arrhenius law for relaxation [60]. Yet our results imply that the nonlinear part can lead to a complex dynamics since for some states and glasses, the relaxation can be slowed down in a power-law fashion for an important number of cages, where the molecules stick for certain orientations. It is also known that this kind of power law also occurs in glasses [60]. The regime where this happens for the softened model and for real glasses is an open problem. Notice that when many rotational traps are present with different relaxation times, stretched exponential laws with special magic exponents are obtained [6,65].

VI. CONCLUSION

In this work we have studied the relaxation process of a chain consisting of three masses joined by nonlinear springs,

periodic conditions, and weakened stiffness. The idea was to explore how relaxation is modified by changes in the low-frequency vibrational mode region. We found that the relaxation time is, for the most part, exponential, which is in agreement with the idea of using an ergodic description. This was confirmed by using a simple flux balance that relates the accessible area of the basin, the initial conditions, and the size of the basin apertures above the saddle points. However, we must stress that the parameter α obtained from the fitting method almost always goes over the α obtained by the flux method (see Fig. 9). Thus, if one were to improve the fit by choosing a smaller time interval, the discrepancies between both methods would increase. In this sense, the flux method is quite useful because it gives a strong insight on what is happening when the initial conditions are evolved. We have shown that by reducing the rigidity of the model, i.e., by softening one of the normal modes, the system relaxes faster. There are two reasons for this. One is the decreasing of the energy barriers since two of the saddle points of the landscape are reduced in energy. The other is related to the shape of the basin. This leads to the conclusion that relaxation occurs mainly into directions of soft or floppy modes [32].

However, we also found some energies and regions in phase space where sticky states appear. For these states, the relaxation decay follows a power law. In these sticky states, the trajectory is quasiperiodic in the sense that, given the isopotential curvature, small deviations occur. Eventually, these deviations are amplified in such a way that the quasiperiodicity is lost and the trajectory goes out of the well. This can also be understood as energy transfer from one normal mode to another. It is believed that the sticky states phase region diminish as the energy increases. However, we have shown that is not always the case and, in fact, there are certain islets in the phase space for which sticky states appear as energy increases (see Fig. 7) and, in fact, it seems nontrivial to understand the relation between energy and sticky states. Having said that, one may not assume that as the energy increases, the sticky states disappear. Furthermore, as the control parameter β, which measures the stiffness of the model decreases, the sticky-states region in phase space diminishes. This is expected since energy sharing (transfer) starts in the low vibrational modes due to resonances. The sticky-states regions were clearly identified with initial conditions for which the assumptions made for the simple flux balance are broken, i.e., regions in which a kind of cavity exist. Therein, for most particles is impossible to leave the energy landscape basin without having many reflections, since their momenta do not have components on the direction of the normal to the lines, which are the gates of the energy landscape basin.

Lastly, we have applied our softened system to model the β relaxation in glasses. We have found that local reorientational jumps can have an exponential and a nonexponential contribution for relaxation, since asymmetric molecules stick in cages for certain orientations. This can help to explain the wide variability observed in the kind of β relaxation [60].

ACKNOWLEDGMENTS

This work was partially supported by Dirección General de Asuntos del Personal Académico-Programa de Apoyo a Proyectos de Investigación e Innovación Tecnológica (DGAPA-PAPIIT) Project No. 102717. J.Q.T.M. acknowledges a doctoral fellowship from Consejo Nacional de Ciencia y Tecnología (México). The authors would like to thank the referees for their comments and inquiries.

[1] K. Trachenko, C. Roland, and R. Casalini, J. Phys. Chem. B **112**, 5111 (2008).
[2] R. Zwanzig, *Nonequilibrium Statistical Mechanics* (Oxford University Press, New York, 2001).
[3] L. Berthier and G. Biroli, Rev. Mod. Phys. **83**, 587 (2011).
[4] P. G. Wolynes and V. Lubchenko, *Structural Glasses and Supercooled Liquids: Theory, Experiment, and Applications* (John Wiley & Sons, New York, 2012).
[5] K. Binder and W. Kob, *Glassy Materials and Disordered Solids: An Introduction to their Statistical Mechanics* (World Scientific, Singapore, 2011).
[6] G. Naumis and J. Phillips, J. Non-Cryst. Solids **358**, 893 (2012).
[7] M. Born, Is classical mechanics in fact deterministic? in *Physics in My Generation* (Springer New York, 1968), pp. 78–83.
[8] M. F. Shlesinger, G. M. Zaslavsky, and J. Klafter, Nature (London) **363**, 31 (1993).
[9] A. Diaz-Ruelas, H. J. Jensen, D. Piovani, and A. Robledo, Europhys. J. Special Topics **226**, 341 (2017).
[10] I. Fermi, P. Pasta, S. Ulam, and M. Tsingou, Studies of the nonlinear problems, Technical Report, Los Alamos Scientific Laboratory, New Mexico, 1955.
[11] A. Ponno, in *Chaotic Dynamics and Transport in Classical and Quantum Systems* (Springer, Berlin, 2005), pp. 431–440.
[12] J. Ford, J. Math. Phys. **2**, 387 (1961).
[13] U. R. Pedersen, L. Costigliola, N. P. Bailey, T. B. Schrøder, and J. C. Dyre, Nature Commun. **7**, 12386 (2016).
[14] S. Albert, T. Bauer, M. Michl, G. Biroli, J.-P. Bouchaud, A. Loidl, P. Lunkenheimer, R. Tourbot, C. Wiertel-Gasquet, and F. Ladieu, Science **352**, 1308 (2016).
[15] H. W. Hansen, B. Frick, T. Hecksher, J. C. Dyre, and K. Niss, Phys. Rev. B **95**, 104202 (2017).
[16] T. Gleim and W. Kob, Europhys. J. B **13**, 83 (2000).
[17] M. Mezard and G. Parisi, in *Structural Glasses and Supercooled Liquids: Theory, Experiment, and Applications* (Wiley, New York, 2012), pp. 151–191.
[18] K. Trachenko and V. V. Brazhkin, Phys. Rev. B **83**, 014201 (2011).
[19] M. Micoulaut and G. Naumis, Europhys. Lett. **47**, 568 (1999).
[20] J. C. Mauro, D. C. Allan, and M. Potuzak, Phys. Rev. B **80**, 094204 (2009).
[21] J. C. Dyre, Rev. Mod. Phys. **78**, 953 (2006).
[22] A. Ninarello, L. Berthier, and D. Coslovich, Phys. Rev. X **7**, 021039 (2017).
[23] G. G. Naumis and R. Kerner, J. Non-Cryst. Solids **231**, 111 (1998).
[24] R. Kerner and G. G. Naumis, J. Phys.: Condens. Matter **12**, 1641 (2000).

[25] J. C. Phillips, J. Non-Cryst. Solids **34**, 153 (1979).
[26] M. Thorpe, J. Non-Cryst. Solids **57**, 355 (1983).
[27] A. Huerta and G. Naumis, Phys. Lett. A **299**, 660 (2002).
[28] A. Huerta and G. G. Naumis, Phys. Rev. B **66**, 184204 (2002).
[29] H. M. Flores-Ruiz and G. G. Naumis, Phys. Rev. E **85**, 041503 (2012).
[30] E. Lerner, G. Düring, and E. Bouchbinder, Phys. Rev. lett. **117**, 035501 (2016).
[31] E. Lerner and E. Bouchbinder, Phys. Rev. E **96**, 020104 (2017).
[32] G. G. Naumis, Phys. Rev. E **71**, 026114 (2005).
[33] G. G. Naumis, Phys. Rev. E **85**, 061505 (2012).
[34] H. M. Flores-Ruiz, G. G. Naumis, and J. C. Phillips, Phys. Rev. B **82**, 214201 (2010).
[35] H. M. Flores-Ruiz and G. G. Naumis, Phys. Rev. B **83**, 184204 (2011).
[36] J. Q. Toledo-Marín, I. P. Castillo, and G. G. Naumis, Physica A **451**, 227 (2016).
[37] J. Q. Toledo-Marín and G. G. Naumis, J. Chem. Phys. **146**, 094506 (2017).
[38] G. G. Naumis, Phys. Rev. B **73**, 172202 (2006).
[39] M. Tatsumisago, B. L. Halfpap, J. L. Green, S. M. Lindsay, and C. A. Angell, Phys. Rev. Lett. **64**, 1549 (1990).
[40] M. Micoulaut and Y. Yue, MRS Bulletin **42**, 18 (2017).
[41] D. Selvanathan, W. J. Bresser, and P. Boolchand, Phys. Rev. B **61**, 15061 (2000).
[42] M. Bauchy and M. Micoulaut, J. Non-Cryst. Solids **357**, 2530 (2011).
[43] A. Ponno, *Chaotic Dynamics and Transport in Classical and Quantum Systems*, Vol. 182 (Springer, Berlin, 2005).
[44] J. Romero-Arias, F. Salazar, G. Naumis, and G. Fernandez-Anaya, Phil. Trans Roy Soc. Lond. A **367**, 3173 (2009).
[45] J. R. Romero-Arias and G. G. Naumis, Phys. Rev. E **77**, 061504 (2008).
[46] M. Onorato, L. Vozella, D. Proment, and Y. V. Lvov, Proc. Nat. Acad. Sci. **112**, 4208 (2015).
[47] I. Limas, G. Naumis, F. Salazar, and C. Wang, Phys. Lett. A **337**, 141 (2005).
[48] G. G. Naumis, Phys. Rev. B **59**, 11315 (1999).
[49] M. Henon and C. Heiles, Astron. J. **69**, 73 (1964).
[50] A. P. Fordy, Physica D **52**, 204 (1991).
[51] J. Aguirre, J. C. Vallejo, and M. A. F. Sanjuán, Phys. Rev. E **64**, 066208 (2001).
[52] B. A. Waite and W. H. Miller, J. Chem. Phys. **74**, 3910 (1981).
[53] M. Toda, *Theory of Nonlinear Lattices*, Vol. 20 (Springer Science & Business Media, Berlin, 2012).
[54] H. J. Zhao and M. L. Du, Phys. Rev. E **76**, 027201 (2007).
[55] W. Bauer and G. F Bertsch, Phys. Rev. Lett. **65**, 2213 (1990).
[56] See Supplemental Material at http://link.aps.org/supplemental/10.1103/PhysRevE.97.042106 for a detailed derivation of the eigenvalues and eigenvectors of the dynamical matrix, as well as a discussion on how we fit $N(t)$ vs t and the graphs, which compare the numerical results $\log[N(t)]$ vs t and the linear fit.
[57] G. G. Naumis, Front. Mater. **2**, 44 (2015).
[58] K. Ngai, *Relaxation and Diffusion in Complex Systems* (Springer Science & Business Media, Berlin, 2011).
[59] Y. H. Liu, T. Fujita, D. P. B. Aji, M. Matsuura, and M. W. Chen, Nature Commun. **5**, 3238 (2014).
[60] H. Tanaka, Phys. Rev. E **69**, 021502 (2004).
[61] H. B. Yu, W. H. Wang, H. Y. Bai, and K. Samwer, Nat. Sci. Rev. **1**, 429 (2014).
[62] G. Diezemann, J. Chem. Phys. **107**, 10112 (1997).
[63] G. Johari, J. Non-Cryst. Solids **307**, 317 (2002).
[64] M. Vogel and E. Rössler, J. Phys. Chem. B **104**, 4285 (2000).
[65] G. G. Naumis and G. Cocho, New J. Phys. **9**, 286 (2007).